Check for updates

Journal of the American Ceramic Society

RESEARCH ARTICLE OPEN ACCESS

Ideal Silicate Glass Compositions: From the Perspective of Network Topology

Erhan Kilinc[1] | Russell J. Hand[2]

[1]Materials and Engineering Research Institute, Sheffield Hallam University, Sheffield, UK | [2]School of Chemical, Materials and Biological Engineering, University of Sheffield, Sheffield, UK

Correspondence: Erhan Kilinc (erhan.kilinc@gmail.com)

Received: 19 June 2026 | **Revised:** 9 October 2026 | **Accepted:** 21 October 2026

Keywords: material properties | molecular bonds | network topology | silicate glasses | spectroscopy

ABSTRACT

The interpretation of commercial soda-lime-silicate and related silicate glass properties through existing topological approaches has received little attention, despite its potential to clarify the relationship between glass chemistry and material properties, including crystallization, physical characteristics, and mechanical behavior. Moreover, robust validation of topological constraint theory in glasses requires a substantial body of experimental data spanning a wide range of structural, mechanical, physical, and physicochemical properties across systematic compositional variations. To address this gap, the number of topological constraints per atom (n_c) was calculated and potential Raman spectral signatures of topological transitions were analyzed for four series of soda-lime-silicate glasses. An exploratory analysis was then conducted to correlate crystallization, physical, mechanical, and structural properties with the resulting topological parameters. The analysis incorporated data from our previous studies and the broader literature to provide a more robust assessment. These topological assessments were complemented by measurements of load- and time-dependent crack growth rates in selected glasses to evaluate their mechanical reliability. The analyses suggest that, beyond the isostatically favorable n_c range, a higher fraction of average six-membered ($m \approx 6$) ring motifs with the established Raman-derived spectral rigidity transition constant (ν_H/ν_M) can serve as effective topological metrics for identifying candidate glass compositions with optimal properties. Overall, these metrics could provide a predictive framework for identifying and refining promising glass compositions without requiring exhaustive characterization across the entire compositional space. Furthermore, the Raman spectral topological signatures identified in soda-lime-silicate glasses can be recognized in quinary silicate and aluminosilicate glass systems, supporting the extension of this framework to related glass networks with comparable structural motifs. This approach may therefore facilitate the development of novel soda-lime-silicate and aluminosilicate glass chemistries tailored to diverse applications.

1 | Introduction

Topological constraint theory provides a framework for understanding the relationships among glass composition, structure, and material properties [1, 2]; it can serve as a powerful tool for designing new glasses with desired properties without the need for extensive experimental trials [3]. This theory can account for composition-property inversions in glass, such as those arising from the boron anomaly or rapid shifts in coordination numbers of boron and aluminum upon compression [3, 4]. It also predicts transitions between stressed-rigid and floppy glass structures based on parameters such as the average coordination number ($< r >$) [5, 6]. Thus, the topological approach enables glass technologists to design glasses by strategically avoiding or

This is an open access article under the terms of the Creative Commons Attribution License, which permits use, distribution and reproduction in any medium, provided the original work is properly cited.
© 2026 The Author(s). *Journal of the American Ceramic Society* published by Wiley Periodicals LLC on behalf of The American Ceramic Society.

leveraging specific structural features or exploiting anomalies to achieve target properties [7].

While the application of topological constraint theory for glass design is a relatively recent development, topological approaches such as cluster theory have previously been used to explain why Pyrex exhibits exceptional resistance to thermal shock and enhanced mechanical resistance [8–10] compared to standard soda-lime-silica glass. More recent studies have identified novel glass chemistries that demonstrate remarkably high crack resistance through the formation of topologically self-adaptive networks [4, 11].

However, the extension of topological constraint theory to conventional soda-lime-silicate glass systems has not yet been fully established. Most relevant studies investigating the relationship between material properties and topological constraint theory have focused on either simple sodium silicate glasses or more compositionally complex silicate glasses, with material properties derived predominantly from molecular dynamics simulations [12–14]. Moreover, the silicate [15] and aluminosilicate glasses [16] display fewer or subtler topological anomalies compared to borosilicate glasses, with some exceptions, such as a notable inversion at 20 mol.% Na_2O in binary Na_2O-SiO_2 glasses [15] or maxima in melt viscosity and some physical properties due to mixed-alkali or alkaline-earth effects [7, 16].

Silicate glasses possess a high energy barrier that prevents Si atoms from reconfiguring to higher coordination states under sharp contact loading [11]. This barrier likely contributes to their low fracture toughness values [17] (0.6–1.0 $MPa{\cdot}m^{1/2}$) and the minimal variation in Poisson's ratio with composition [18]. In contrast, resistance to static fatigue can vary substantially among compositions, even when fracture toughness and elastic moduli values are similar [19, 20], making it a meaningful metric of the long-term strength of glass. However, the exact link between stress corrosion and glass composition remains largely unknown and debated [21], and a notable gap persists in the literature regarding the specific influence of topological properties on stress-corrosion in silicate and commercial soda-lime-silica glasses.

In this study, we aim to interpret variations in the measured properties of 25 silicate glasses by applying different topological approaches, integrating theoretical analysis with previously published experimental data for these glasses [22, 23]. These datasets include XRF chemical analysis, crystalline phase fields, bulk crystal growth rates obtained through Rietveld refinement of XRD patterns, and network connectivity derived from Raman spectroscopy and ^{29}Si NMR, as well as mechanical properties such as Vickers hardness, flexural strength, brittleness, and elastic moduli. To complement these datasets, DSC measurements were carried out in the present study to provide further calorimetric insight into glass transition behavior. In addition, indentation experiments were performed to evaluate the cracking and static fatigue properties of selected glasses, with particular consideration given to the high sensitivity of this method to atmospheric humidity, especially under applied stress [20].

The complementary topological information for exploring the topological sensitivity of the material properties of the studied glasses was obtained using Raman scattering. Topological variations, including ring-size distributions in silicate glasses as a function of composition, have previously been investigated by Zhou et al. [24] using neutron diffraction and computational simulations. Although these approaches can provide detailed and quantitative insights into the structural topology of silicate glasses, Raman scattering offers a more readily accessible spectroscopic approach for probing topological features and transitions. While Raman spectroscopy may not provide the same level of structural resolution as neutron diffraction and simulation-based approaches, it can nevertheless provide valuable information on ring-size distributions and other topological characteristics [25, 26].

Moreover, Raman vibrational features have also been considered as structural descriptors for correlating molecular configuration with material properties by Cassetta et al. [27] and Pan et al. [28]. Their studies primarily focused on variations in material properties associated with changes in the characteristics of the Raman boson band. Cassetta et al. [27] demonstrated that the boson band provides a sensitive spectroscopic probe of nanoscale structural heterogeneity, linking low-frequency vibrational dynamics to the physical and rheological properties of glassy materials. Similarly, Pan et al. [28] showed that the boson band serves as a spectroscopic fingerprint of elastic heterogeneity in glasses, with its frequency and intensity correlating with the characteristic length scale of rigidity fluctuations, Poisson's ratio, and liquid fragility.

In the present study, we calculated the average number of rigid constraints per atom (n_c) based on the methodologies reported in the literature, while Raman spectral features beyond the boson-peak region were processed and analyzed alongside the n_c values to identify property domains in which significant spectral signatures of topological transitions coincide with anomalies in the measured glass properties. Finally, an exploratory analysis was conducted to investigate the potential interrelationships and underlying mechanisms linking various material and topological properties, with the aim of identifying ideal glass networks. Where applicable, this analysis, as with the variation in liquidus temperature with n_c, was further extended by incorporating relevant data from the literature to examine these interrelationships across a broader range of soda-lime-silicate and aluminosilicate compositions. Overall, the potential for identifying ideal glass networks was assessed by examining the relationships between the diverse measured material and structural properties in relation to the topological criteria proposed [9, 29] for ideal silicate glass networks.

2 | Methodology

2.1 | Design of Composition

The main study focuses on four glass series comprising a total of 25 soda-lime-silicate glasses, with all series sharing the same underlying soda-lime-silicate composition. Their coded names, as used in our previous publications [22, 23], are reiterated here as MS, CS, ASN, and MC to enable traceability of previously reported property data. This study does not explicitly consider the role of individual oxide components; instead, it focuses on the influence of topological variations on the material properties of glasses.

15512916, 2026, 11, Downloaded from https://ceramics.onlinelibrary.wiley.com/doi/10.1111/jace.71368 by University Of Sheffield, Wiley Online Library on [03/11/2026]. See the Terms and Conditions (https://onlinelibrary.wiley.com/terms-and-conditions) on Wiley Online Library for rules of use; OA articles are governed by the applicable Creative Commons License

The general formula for the MS glass series is $(75 - y)$ $SiO_2{\cdot}13.5Na_2O{\cdot}10CaO{\cdot}(y)$ $MgO{\cdot}1.5Al_2O_3$ (mol.%) where $y = 0$, 1, 2, 3, 4, 5, 6, 7 (glasses coded as $M_yS_{(75-y)}$). The CS glass series is defined by $(75 - x)SiO_2{\cdot}13.5Na_2O{\cdot}(7 + x)CaO{\cdot}3MgO{\cdot}1.5Al_2O_3$ (mol.%) where $x = 0, 1, 2, 3, 4, 5, 6, 7$ (glasses coded as $C_{(7+x)}S_{(75-x)}$).

The ASN series follows the general formula $(75 - 2w)$ $SiO_2{\cdot}$ $(12 + w)$ $Na_2O{\cdot}10CaO{\cdot}3MgO{\cdot}wAl_2O_3$ (mol.%) where $w = 0$, 0.5, 1.5, 2.5, 3.5 and 4.5. In the MC series, the ratio of CaO to MgO was varied while all other constituents were held constant; its general formula is: $72SiO_2{\cdot}13.5Na_2O{\cdot}$ $(13 - z)$ $CaO{\cdot}(z)MgO{\cdot}1.5Al_2O_3$ (mol.%) where $z = 1$, 3, 5, 7, 9, and 11.

2.2 | Previously Measured Glass and Material Properties

Our previously published parent studies detailed the procedures used for measuring the chemical composition [22, 23], density [23], crystalline phase field [23], bulk crystal growth rate [23], liquidus temperature [23], Vicker's hardness [22, 23], elastic moduli [23], Poisson's ratio [22, 23], flexural toughness [23], brittleness [23] and the connectivity data from Raman [22, 23] and ^{29}Si NMR studies [22] along with the numerical results obtained.

As the topologically relevant spectral data provide the foundation for the discussion presented here, the corresponding methodology is briefly reiterated below. Raman spectra were acquired from polished solid glass specimens (3 × 20 × 20 mm) using a Renishaw In Via Raman spectrometer equipped with a CCD detector. Measurements were performed using an excitation wavelength of 514.5 nm, with the laser beam delivered through a ×50 objective, a laser power of 20 mW, and an acquisition time of 10 s. The spectrometer was calibrated against silicon before each measurement session. Spectra were collected over the range of 0–1500 cm^{-1} with a spectral resolution of 1 cm^{-1}.

Notably, among these background data, those most sensitive to topological variations are explicitly presented in Section 3, while the remaining data are used to support and contextualize the overall interpretation concisely.

2.3 | Newly Measured Material Properties

2.3.1 | Stress-Corrosion Susceptibility

Indentation cracking may be distinctive, as it can greatly differ for different glass systems; therefore, indentation can be used to probe crack initiation load or crack formation probability as well as the type of deformation in glass under sharp contact loading [30]. Unless indentation is conducted in a dry, atmosphere-controlled chamber, stress-corrosion-driven crack growth will occur following indentation; therefore, immediate post-indentation measurements will minimize such environmental effects. In contrast, extended measurements taken 24 h later will be affected by crack growth driven by stress corrosion. Therefore, 24-hour indentation data provide additional insights into the combined influence of water species and glass chemical composition on the crack behavior of silicate glasses under static stresses.

Indentation-based stress corrosion studies were conducted on the MS and CS glass series. Indentation test specimens (3 × 20 × 20 mm) were obtained from the main cast glass blocks (60 × 20 × 20 mm in dimension) of these glass series and were subjected to post-annealing after machining and polishing. Details of the sample specifications and fabrication procedures are provided in background studies [22, 23]. Indentation studies were carried out in ambient air at 24 ± 1°C with a relative humidity of approximately 60%, and the total length of radial cracks ($2c_0$) emanating from the corners of the indents was measured immediately after indentation. Subsequently, the total crack length ($2c_{24}$) was measured again 24 h post-indentation to determine the crack extension for each indent. The dependence of stress corrosion on n_c is examined using the crack growth data, $\Delta c = c_{24} - c_0$, obtained at an indentation load of 49.05 N with a dwell time of 20 s.

2.3.2 | Glass Transition Range Analysis

Differential thermal analysis was conducted using a PerkinElmer Pyris 1 TGA instrument to analyze the glass transition region of the four glass series studied. Finely ground powder samples (<75 μm) were heated to 1000°C at a rate of 10°C/min, cooled to room temperature at the same rate, and then reheated to 1000°C at 10°C/min. The glass transition temperatures were determined from the second heating curve using the built-in Perkin-Elmer software. For the glass transition, both the onset temperature of the glass transition (T_o) and the end temperature of the glass transition region (T_e) were identified based on the method described by Ojovan [31].

2.3.3 | Raman Scattering Analysis

The main low-frequency band of the Raman spectra, after intensity normalization and baseline subtraction, was analyzed to determine the ring-size distribution within the network of the studied glasses. Gaussians were used for spectral curve fitting without initially constraining parameters such as position (v), bandwidth, or intensity. The fitting process aimed to minimize the number of Gaussians while capturing physically plausible structural features. Four Gaussians were found sufficient; detailed justification for their assignment to specific ring motifs is provided below (see Section 3). The quality of the fit was assessed by examining the squared residual between the sum of the fitted peaks and the original spectrum. The area under each Gaussian was calculated to quantify its contribution to the main structural band. The relative abundance of these peaks was then used as a metric to determine the ring-size distribution, offering insights into the structural characteristics of the studied glasses.

3 | Results and Discussion

3.1 | The Concept of Ideal Glass Network and Topology

Phillips and Kerner [9], Bauchy et al. [14], and Laurent et al. [29] argued that an isostatic (stress-free) glass network, where each atom experiences an average of three rigid constraints ($n_c = 3.0$),

15512916, 2026, 11, Downloaded from https://ceramics.onlinelibrary.wiley.com/doi/10.1111/jace.71368 by University Of Sheffield, Wiley Online Library on [03/11/2026]. See the Terms and Conditions (https://onlinelibrary.wiley.com/terms-and-conditions) on Wiley Online Library for rules of use; OA articles are governed by the applicable Creative Commons License

is optimal for attaining ideal mechanical, physical, and chemical properties in glass. Although the criteria for an ideal glass network are subjective and may depend on the specific application or field of glass science, in this study, an ideal glass network refers to a glass network that may exhibit a lower tendency toward crystallization, together with improved mechanical performance and enhanced resistance to static fatigue. Furthermore, Phillips and Kerner [9] introduced the complementary criterion of ring-size distribution to achieve an isostatic network and identify ideal glass compositions. They noted that a combination of $m = 6$ ring motif statistics and $n_c = 3.0$ leads to an ideal composition of $74SiO_2$-$16Na_2O$-10CaO (wt.%). However, this composition is not unique, and the alternative ideal silicate glass compositions proposed by Laurent et al. [29], derived from molecular dynamics simulations, also satisfy the topological constraint of $n_c = 3.0$. These compositions extend from the SiO_2 apex to the midpoint of the Na_2O-CaO edge in the SiO_2-Na_2O-CaO phase diagram. It is worth noting, however, that while these compositions may meet at least one of the proposed topological constraints, they do not necessarily exhibit the technological and processing properties typical of commercial soda-lime-silica glasses.

In this study, the n_c values were calculated based on the proposed approaches of Phillips and Kerner [9] and Liu et al. [32]. The number of bond-stretching (BS) and/or bond-bending (BB) constraints created by Si, Na, and Ca were based on the work of Laurent et al. [29], while the total number of rigid constraints for Mg was assumed to be identical to that for Ca. In line with the molecular dynamic simulation-driven BS and BB calculations of Laurent et al. [29], the total number of BS + BB constraints for four-coordinated aluminum (Al) atoms was taken to be 7, following the work of Ching and Bauchy [33]. Accordingly, the average number of topological constraints per atom, n_c, is calculated as follows:

$$n_c = \frac{\left(\sum_i x_i n_i\right)}{\left(\sum_j x_j N_j\right)} \tag{1}$$

where the summations are taken over all species, i, and oxide components, j, respectively. Here, x_i is the mole fraction of species i, n_i is the number of rigid constraints contributed by species i, and N_j is the number of atoms in oxide component j. The species considered in the present model are Si, Na, Ca, Mg, Al, bridging oxygen (O_{BO}), and non-bridging oxygen (O_{NBO}). The values of N are 3 for SiO_2, 5 for Al_2O_3, 2 for CaO and MgO, and 3 for Na_2O, while x_j denotes the mole fraction of oxide component j. The total oxygen content is given by:

$$O_{Total} = O_{BO} + O_{NBO}$$

where the concentration of O_{NBO} is calculated as:

$$O_{NBO} = 2x_{Na2O} + 2x_{CaO} + 2x_{MgO} - 2x_{Al2O3}$$

and the total oxygen content is:

$$O_{Total} = 2x_{SiO2} + x_{Na2O} + x_{CaO} + x_{MgO} + 3x_{Al2O3}.$$

The uncertainty in n_c was determined using the quotient rule for error propagation, which accounts for functions containing shared variables in both the denominator and numerator. This involved determining the partial derivatives of n_c with respect to the fractional molar content of each constituent. The uncertainties in n_c were derived from the uncertainty values associated with the major and minor oxide components in the studied glasses, which were obtained from the measurement errors of the corresponding XRF analyses reported in our previous work [23]. These uncertainties were then propagated to n_c using standard error-propagation methods.

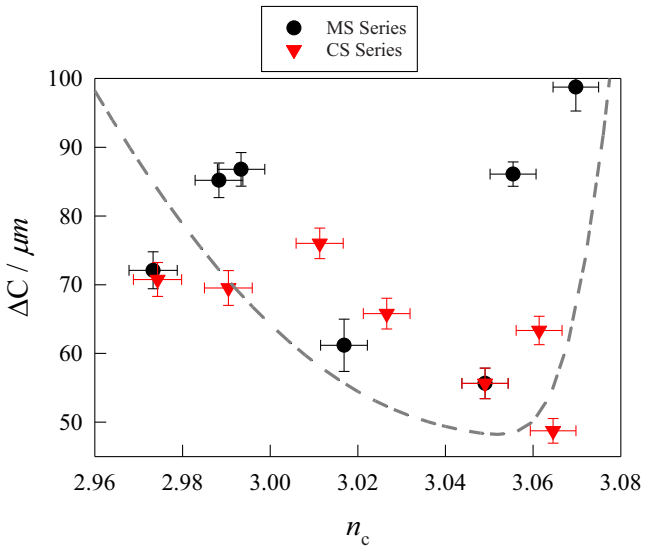


FIGURE 1 | Variation of crack growth as a function of n_c in the studied glasses. The error (Δ) formula of crack growth (ΔC) is, $\sigma_{\Delta C} = \sqrt{(\sigma_{C_{24}})^2 + (\sigma_{C_0})^2}$.

Our calculated n_c values for the studied glasses using the Phillips and Kerner [9] and Ching and Bauchy's [33] approaches align closely, with a maximum standard deviation of ± 0.01. The n_c values range from 2.92 to 3.11, corresponding to the glasses with the lowest and highest degree of polymerization, respectively, across the four studied glass series. These results suggest that soda-lime-silicate glass compositions relevant to industrial processing exhibit n_c values comparable to those reported by Phillips and Kerner [9] and Laurent et al. [29] for ternary and ideal Na_2O-CaO-SiO_2 glasses. Notably, the quinary silicate glasses investigated here, which closely resemble commercial soda-lime-silica glasses, cluster around the isostatic network region, with n_c values ranging from 3.0 to 3.06.

3.2 | Crack Growth and n_c

Figure 1 shows crack growth as a function of n_c for the two glass series studied. Stress corrosion-driven crack growth decreases as n_c increases from 2.97 to 3.05. Around $n_c = 3.05$, the cracks begin to deflect, and crack growth increases again for $n_c > 3.05$. Although the indentation fracture toughness of these glasses varies little with composition or n_c, crack growth varies substantially across the studied n_c range. Specifically, crack growth decreases by nearly half between the lowest n_c and $n_c = 3.05$, then nearly doubles as n_c reaches its maximum value. This trend suggests a potential influence of network topology on the static fatigue behavior of soda-lime-silicate glasses. A similar trend is

15512916, 2026, 11, Downloaded from https://ceramics.onlinelibrary.wiley.com/doi/10.1111/jace.71368 by University Of Sheffield, Wiley Online Library on [03/11/2026]. See the Terms and Conditions (https://onlinelibrary.wiley.com/terms-and-conditions) on Wiley Online Library for rules of use; OA articles are governed by the applicable Creative Commons License

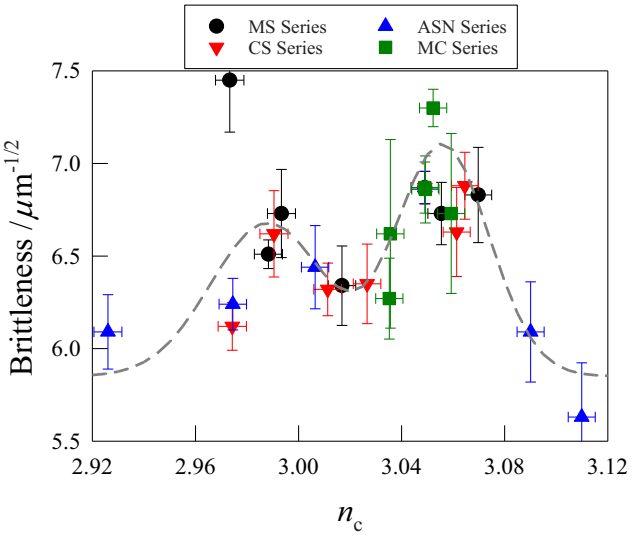


FIGURE 2 | Measured brittleness versus calculated n_c for the studied glasses. The error (Δ) formula of brittleness (B) is $\frac{\Delta B}{B} = \sqrt{\left(\frac{\Delta H}{H}\right)^2 + \left(\frac{\Delta K_{IC}}{K_{IC}}\right)^2}$.

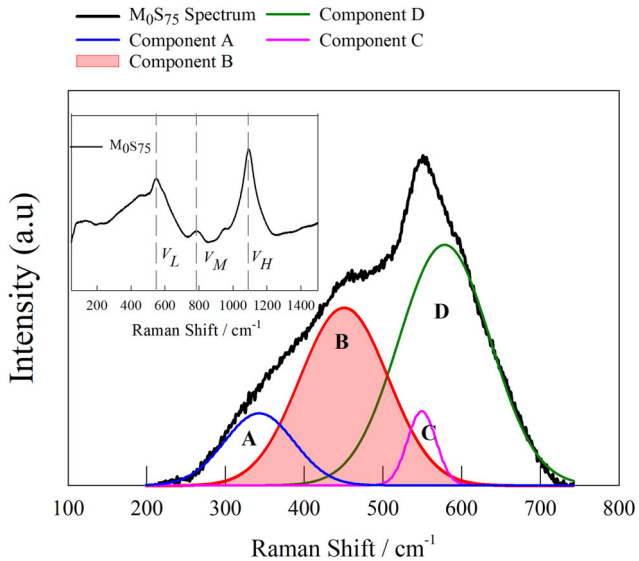


FIGURE 3 | Examples of bending vibrational mode components within the main low-frequency Raman band. The inset shows the centroid positions of ν_L, ν_M, and ν_H for the three main Raman scattering bands in the raw spectrum of the M_0S_{75} glass.

observed for brittleness, defined as the ratio of Vickers hardness to flexural fracture toughness, which also exhibits a local minimum within the isostatic region, corresponding to an n_c range of 3.00–3.05 (Figure 2). It is important to note that mechanical properties such as static fatigue and brittleness in glasses are highly complex and difficult to predict, as they cannot be strongly correlated with any single compositional, structural, or physical parameter. Nevertheless, the observed minima in stress-corrosion resistance at approximately $n_c = 3.05$ and in brittleness at $3.00 < n_c < 3.05$ underscore the potential role of the rigidity transition in influencing these particularly unpredictable properties.

3.3 | Raman Scattering Ring-Size Distribution

3.3.1 | Assignment of the Vibrational Modes

As shown in our earlier study [22], the network connectivity data for the studied soda-lime-silicate glass systems—including the Raman scattering polymerization index, the fractions of Q^4 and Q^3 motifs determined by ^{29}Si NMR, and the physical and elastic properties—vary approximately linearly with composition. However, such linear trends do not extend to the relative intensities of certain major structural features in the low-frequency region of the Raman spectra. Our previously published clustered Raman scattering analysis of these glasses [23] showed that the relative intensities of the spectral feature near ~590 cm^{-1} and the feature at ~480 cm^{-1}, which generally exhibits plateau behavior, are highly sensitive to compositional variations.

As shown in Figure 3, deconvolution of the main low-frequency Raman band identified four primary components across the four glass series, with approximate peak positions ranging from ~325 to 375 cm^{-1} (A), ~445 to 485 cm^{-1} (B), ~540 to 590 cm^{-1} (C), and ~560 to 655 cm^{-1} (D). Notably, the relative intensity of the largest Gaussian component B, centered between ~445 and 485 cm^{-1}, exhibits a nonlinear variation with composition in each glass series, despite the approximately linear network depolymerization observed over the same compositional range.

3.3.2 | Origin of Rings Structures in Silicate Glasses

The Raman scattering patterns of silicate glasses change with the progressive replacement of the main band of fused SiO_2 at 430 cm^{-1} by a series of higher-frequency bands as modifiers are added [34]. The computational studies by Barmes et al. [35] and Shiga et al. [36] indicate that six-membered rings are the most prevalent ring motifs in vitreous silica, contributing to the characteristic Raman scattering band centered at around 430 cm^{-1}, and the morphology of this band evolves with frequency shifts greatly with a number of factors such as glass chemistry, irradiation, or applied pressure [25]. Such changes are expected as variations in the average Si-O-Si bond angle distribution and bond force constants; for instance, an angle disparity of approximately 4° can lead to a major shift of about 100 cm^{-1} in the ring motif positions within the same glass system [37].

Awazu et al. [26] demonstrated that the vibrational Raman mode frequencies and relative mode intensities of five-, six-, eight-, and higher-membered rings are sensitive to high-energy irradiation. They also reported an inverse, linear-like relationship between the size of the ring motifs and the vibrational frequency in silica glass. Furthermore, in depolymerized aluminosilicate glass systems, Le Losq et al. [38] reviewed the origins and approximate positions of different ring motifs, drawing on relevant background studies, and showed that bands extending from 250 to 480 cm^{-1} are typically associated with the spectral signatures of tetrahedral units within five-, six-, seven-, or larger-membered rings in aluminosilicate glasses.

Consistently, components A and B, located at the lower-frequency end of the spectrum, appear to correspond primarily to vibrational modes associated with six- and larger-membered ring

15512916, 2026, 11, Downloaded from https://ceramics.onlinelibrary.wiley.com/doi/10.1111/jace.71368 by University Of Sheffield, Wiley Online Library on [03/11/2026]. See the Terms and Conditions (https://onlinelibrary.wiley.com/terms-and-conditions) on Wiley Online Library for rules of use; OA articles are governed by the applicable Creative Commons License

motifs in the soda-lime-silicate glasses examined. Computational analysis has also shown that the maximum m values for ring motifs in simple alkali silicate glasses are around nine [39]. Thus, vibrational modes associated with rings with $6 < m < 9$ are considered to contribute to the intensity of component A at the lower end of the vibrational spectrum, whereas component B is more likely to be associated predominantly with ring motifs having an average ring size of approximately six. Component D, on the other hand, can be assigned to vibrations associated with smaller ring motifs ($m < 6$), specifically three-, four-, and five-membered rings within the compositional range studied (Figure 3), and is situated at the higher-frequency end of the vibrational spectrum. Overall, in our study, component B can reasonably be attributed predominantly to vibrational modes associated with six-membered ring motifs, and the relative intensities of these components were used as indicators of variations in the populations of different ring motifs in the soda-lime-silicate glasses.

3.3.3 | Ring-Statistics Versus n_c and (ν_H/ν_M)

We conducted an exploratory analysis to investigate potential correlations between vibrational mode frequencies and the n_c in the studied glasses. As a simplified approach, we analyzed the central Raman shifts (centroids)—denoted as ν_L, ν_M, and ν_H—corresponding to the low-, mid-, and high-frequency bands, respectively, rather than isolating their topologically sensitive vibrational components. Further details, including the positions of these Raman vibrational bands, can be found in the inset of Figure 3.

The Raman bands in the vicinity of ν_H in soda-lime-silicate glass systems have typically been assigned to symmetric Si-O stretching motions of depolymerized silicate units, comprising SiO_4 tetrahedra with one, two, three, and four non-bridging oxygens, respectively [34, 40]. These modes therefore have a predominantly intra-tetrahedral character. In contrast, the vibrational mechanisms associated with the lower-frequency bands involve increasingly significant contributions from motions of the Si-O-Si linkages. The ν_M band has been attributed to a combination of Si-O-Si bending and Si-O stretching motions [41, 42, 43], whereas the ν_L band is predominantly associated with bending motions of the Si-O-Si linkages [41]. Thus, with decreasing Raman scattering frequency from ν_H to ν_M and ν_L, the vibrational character evolves from predominantly intra-tetrahedral Si-O stretching to increasingly dominant inter-tetrahedral bending motions involving the Si-O-Si linkages.

Our exploratory analysis indicated that, although there is no strong one-to-one correlation between ν_L, ν_M, or ν_H and n_c; the centroid of the mid-frequency band (ν_M) exhibits a relatively linear blueshift with increasing n_c, with a subtle minimum around $n_c = 3.06$. In contrast, although the frequencies of the intramolecular stretching modes also vary significantly with n_c, they do not exhibit a clear systematic trend. However, introducing the spectral rigidity transition parameter, ν_H/ν_M, and examining its variation with n_c reveals an intriguing pattern that can be reasonably linked to the concept of Maxwell isostatic criterion. As shown in the top view of Figure 4, the ν_H / ν_M ratio reveals a more distinct and informative pattern compared to the individual frequency shifts. Specifically, this ratio initially decreases sharply

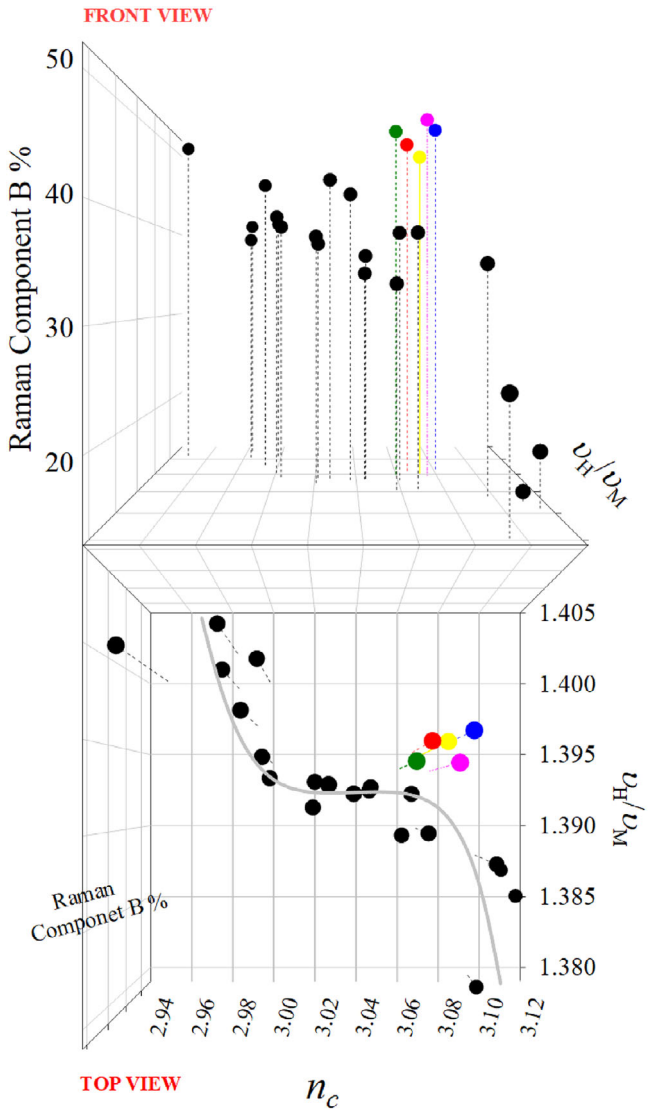


FIGURE 4 | 3D plots showing the variation of Raman Component B (%) with the ν_H/ν_M ratio and n_c in the studied glasses, viewed from the front and the top, respectively.

as n_c increases, then levels off into a plateau as the system enters the isostatic region ($3.0 < n_c < 3.06$). It subsequently rises at $n_c \approx 3.06$ for the color-coded data points, before declining again as the network transitions into the over-constrained phase.

The front and top views of Figure 4 also show how component B varies with ν_H / ν_M and n_c, respectively, within a three-dimensional space for the studied glasses. The proportion of component B shows an inverse, nearly linear trend with increasing n_c values, indicating that the population of average $m \approx 6$ ring motifs decreases as the network's stress-rigidity increases. Notably, the glasses with the highest fractions of average $m \approx 6$ ring motifs are clustered around $n_c = 3.06$ and are shown in different colors for easier identification. This surge in $m \approx 6$ ring motifs may reflect the network's proximity to the rigidity transition, where the system approaches isostatic conditions. At this stage, ring types are likely reorganized into topologically ideal $m \approx 6$ motifs, which may provide an efficient balance among different types of network constraints before stress-rigidity effects

15512916, 2026, 11, Downloaded from https://ceramics.onlinelibrary.wiley.com/doi/10.1111/jace.71368 by University Of Sheffield, Wiley Online Library on [03/11/2026]. See the Terms and Conditions (https://onlinelibrary.wiley.com/terms-and-conditions) on Wiley Online Library for rules of use; OA articles are governed by the applicable Creative Commons License

become dominant. For n_c values above 3.06, the decline in the $m \approx 6$ ring population becomes much steeper as the network progressively enters the stress-rigid phase. Collectively, these observations suggest a reciprocal relationship between the nature of the phase fields and the evolution of ring statistics.

3.4 | Detailed Overview of Spectral Signatures

Micoulaut et al. [42] previously investigated topological transitions in CaO-SiO_2 glasses using Raman scattering as a structural probe. They identified several characteristic vibrational modes across the low-, mid-, and high-frequency regions, which were found to be highly sensitive to topological changes occurring during the transition from the stressed-rigid to the floppy phase. Notably, the mode observed in the mid-frequency region was attributed to inter-tetrahedral bending (angular) motions of Si-O-Si linkages and was considered highly sensitive to the rigidity transition. In the high-frequency region, the most prominent vibrational mode was associated with the intra-tetrahedral stretching vibrations of Q^n species within the silicate glass network.

In silicate glasses, angular modes are weaker than BS modes [40], as reflected by their occurrence at lower Raman frequencies. Consequently, the initial rebound of the ν_H/ν_M ratio to higher values around $n_c = 3.06$, followed by a subsequent decrease, suggests the presence of an isostatic sub-region in which inter-tetrahedral angular constraints may undergo re-softening, while intra-tetrahedral stretching constraints associated with Q^n species simultaneously re-stiffen. A similar re-softening behavior was reported by Boolchand et al. [44] in binary Ge-Se glasses, where the vibrational frequency of corner-sharing modes increased super-linearly with increasing network rigidity, except for a distinct sub-linear dependence within the isostatic region. This behavior is consistent with the near-constant ν_H/ν_M ratio observed between $n_c = 3.00$ and 3.06, suggesting that the re-softening of angular vibrational modes becomes pronounced within the isostatic regime.

This behavior may be attributed to a self-organization mechanism that either maintains the glass in an isostatic state [45] or delays its rapid departure from the isostatic region near $n_c = 3.0$. Our previous ^{29}Si NMR analysis of selected samples from these glass series [22] indicated that their networks consist predominantly of Q^4 and Q^3 species. The concurrent hardening of intra-tetrahedral stretching modes (higher ν_H) and the softening of inter-tetrahedral angular modes (lower ν_M) within these structural units parallels the topological evolutions observed in the CaO-SiO_2 glass system. In that system, the inter-tetrahedral angular modes exhibit plateau-like behavior as the network becomes increasingly polymerized and n_c increases with increasing SiO_2/CaO molar ratio, followed by pronounced softening toward the SiO_2-rich end. Notably, a locally sharp softening of these modes also occurs within the plateau region, coinciding with the rigidity-transition threshold in this glass system. A similar behavior is observed across the four glass series studied here: the glasses clustered around $n_c = 3.06$, which also exhibit the highest abundance of $m \approx 6$ rings, show the locally largest ν_H/ν_M ratios. This combination suggests a greater capacity for inter-tetrahedral flexibility within the network while the overall network shifts toward the stressed-rigid phase field. Consistent with this interpretation, simulation studies [46] have shown that increasing the proportion of flexible angular bonds between rigid tetrahedra enhances nano-ductility, toughness, and the glass-forming ability in aluminosilicate glasses. Therefore, the local reversibility of inter-tetrahedral flexibility as network domains stiffen may present a characteristic feature of topologically ideal silicate networks.

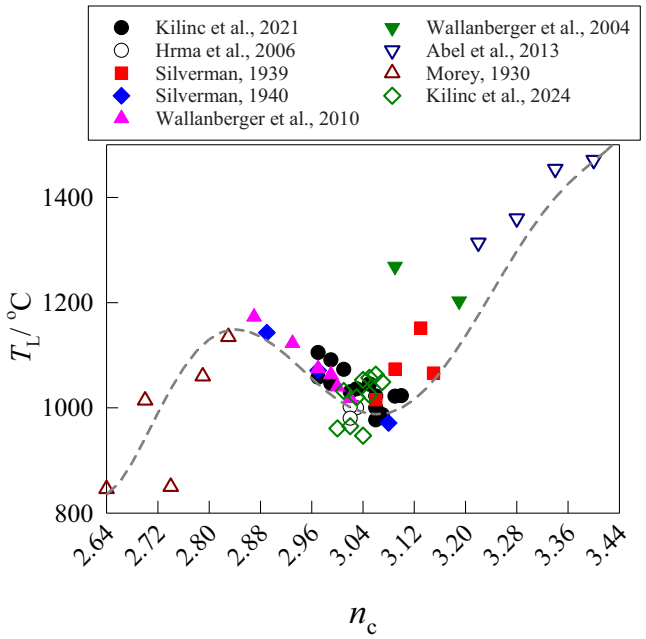


FIGURE 5 | The association between liquidus temperature and n_c from a broader perspective, incorporating various subsets of silicate glass systems from both literature and our studies. The maximum magnitude of the measurement error is assumed to be ±10°C, which is small compared to the scale of variation in the dataset and does not affect the observed trend; consequently, the error bars are not included here.

3.5 | Liquidus Temperature—Network Topology

Glasses with an ideal, isostatic network have also been shown to exhibit improved crystallization properties and glass-forming ability, as reported by Sharmila et al. [5] and Varma et al. [6]. The requirement that the liquidus temperature be lower than the glass-melt processing temperature is an important consideration in glass composition design. However, there are currently no robust empirical models for predicting crystallization properties, such as liquidus temperature, and these properties cannot be reliably correlated with any single fundamental glass property. Therefore, identifying significant associations between the crystallization properties of soda-lime-silicate glasses and their topological signatures or variants may provide insight into the underlying relationship between glass network topology and crystallization behavior.

Figure 5 shows the broader variation of liquidus temperature, extending our analysis of selected glasses from this study by incorporating literature data [47–54] on glasses rich in either network formers (SiO_2, Al_2O_3) or network modifiers (CaO, MgO,

15512916, 2026, 11, Downloaded from https://ceramics.onlinelibrary.wiley.com/doi/10.1111/jace.71368 by University Of Sheffield, Wiley Online Library on [03/11/2026]. See the Terms and Conditions (https://onlinelibrary.wiley.com/terms-and-conditions) on Wiley Online Library for rules of use; OA articles are governed by the applicable Creative Commons License

Na_2O) to explore the relationships between liquidus temperature and network topology in silicate glasses. The details of the extracted liquidus temperature and composition data used to construct Figure 5 can be found in Kilinc et al. [23] for the MS and CS data series and in Kilinc et al. [54] for the T1-T4 and C1-C6 datasets, respectively.

The glass compositions sourced from Wallenberger and Smrček [52] (coded 1–6 on p. 155) are quinary soda-lime-silicate glasses and exhibit significant variations in the SiO_2/CaO ratio, including unusually low SiO_2 contents of down to 62.18 mol.%. Similarly, the glass compositions containing 14.8 and 16.25 wt.% Al_2O_3 (Tables 2 and 3, respectively, in the source paper) belong to the SiO_2-CaO-Al_2O_3 system reported by Wallenberger et al. [50], where the molar difference (CaO-Al_2O_3) is greater than zero, assuming that aluminum is present in four-fold coordination. The glass compositions sourced from Abel et al. [53] generally exhibit higher SiO_2 contents and slightly lower Al_2O_3 contents within the SiO_2-CaO-Al_2O_3 system than those reported by Wallenberger et al. [50].

The glasses reported by Hrma et al. [51] are representative commercial float-glass compositions (coded CMA1, CLA1, and B-HNa in the source paper). Compared with typical float-glass compositions, these glasses contain lower Na_2O and CaO contents, higher SiO_2 and MgO contents, and, more importantly, negligible Al_2O_3 contents. The glass data sourced from Silverman [48] (coded 63 and 64 in the source paper) are MgO-free compositions within the quaternary soda-lime-silica glass system. In contrast, the glasses sourced from Silverman [49] dataset belong to a quinary glass system and contain significantly higher MgO and lower SiO_2 contents than most archetypal soda-lime-silica glass compositions. Furthermore, the compositional data sourced from Morey [47] comprise glasses from the SiO_2-Na_2O-CaO ternary glass system, with significantly higher Na_2O contents ranging from approximately 17 to 32 mol.%.

Consistently, Figure 5 shows a pronounced minimum in the liquidus temperature of number of glass systems that collected from literature including some of our studied silicate glasses at $n_c \approx 3.06$ within the isostatic region. However, n_c may not be the sole factor that contributing to the liquidus position of these glasses. Notably, this minimum tends to coincide with a higher abundance of $m \approx 6$ ring motifs, at least within our studied four glass series. Moreover, our XRD study [23] of an extended heat-treated four-glass series indicated that the primary crystalline phase shifts from silica (cristobalite and tridymite) to wollastonite at this intersection point, where the ν_H/ν_M ratio becomes more balanced, as inferred from Figure 4.

It is well established that ternary soda-lime-silica glasses with high Na_2O contents exhibit some of the lowest liquidus temperatures among soda-lime-silicate glass systems, although these glasses typically do not possess the desirable physical, rheological, and technological properties of commercial soda-lime-silica glasses. One would therefore expect the addition of alkaline earth oxides and alumina, as found in conventional quinary soda-lime-silica systems, to significantly increase the liquidus temperature as the n_c value increases. This increase would be expected to continue, and potentially become disproportionate, toward compositions characteristic of E-glass systems (the CaO-Al_2O_3-SiO_2 system, with cristobalite and anorthite phase fields, as indicated in the parent studies [50, 53]) within the stressed-rigid region.

Overall, it would be plausible to assume that the variation in liquidus temperature would increase at least linearly, if not non-linearly, with increasing n_c values between $n_c = 2.6$ and 3.5. Conversely, as the glass compositions move toward the commercially viable soda-lime-silica glass system, where the n_c values concurrently approach ~3.06, the liquidus temperature appears to reverse toward a local minimum before subsequently returning toward the expected liquidus-temperature values at higher n_c. This observation indicates that the non-linear variation, or local minimum, in liquidus temperature is unlikely to arise from random variation. Instead, it reinforces the potential influence of the ideal glass-forming region on glass properties near $n_c = 3.0$. It also strongly suggests that the observed trend is likely to remain robust even with the addition of further data points across the $n_c = 2.6$–3.5 range.

In addition to the pronounced minimum in liquidus temperature observed at around $n_c \approx 3.06$, the extended bulk devitrification study-based on the glasses examined and detailed in Kilinc et al. [23], indicating that the percentage of the amorphous phase reaches its highest values when the n_c value of the glass series approaches 3.06 expect for two outliers. Overall, extending the liquidus temperature dataset across a wider n_c spectrum provides a more comprehensive and explicit view of the influence of the topologically ideal silicate glass region on the liquidus temperature of glasses.

3.6 | Glass Transition Region—Network Topology

No signs of crystallization were observed in the glasses studied under the applied heating and cooling during thermal analysis. Neither the glass transition temperature (T_g) nor the width of the glass transition range (T_e–T_o) shows a clear association with n_c. On the other hand, as shown in Figure 6, the end temperature of the glass transition (T_e) exhibits a distinct non-linear dependence on n_c for the studied glass series, reaching peak values around $n_c = 3.04$. Note that T_e is an operational parameter whose numerical value is intrinsically tied to thermal history and the cooling or heating rates employed during measurement. These effects were eliminated by erasing prior thermal history using the second heating curve and applying identical heating and cooling rates for all glasses presented in Figure 6. The difference between the lowest and highest measured T_e values is nearly 20°C, marking a significant variation across the studied compositional space.

Optimally constrained networks ($n_c \approx 3.0$) form strong glass-forming liquids [55, 56] and are known to exhibit lower thermal hysteresis and smoother structural relaxation [56, 57]. In contrast, under-constrained and over-constrained networks tend to deviate substantially from the thermodynamic equilibrium path near the glass transition during cooling, resulting in poorer structural relaxation and greater thermal hysteresis upon reheating [56]. These behaviors likely contribute to lower percolation thresholds [31] and reduced glass transition temperatures. Notably, a positive slope in T_g with increasing mean coordination number <r> has been observed in chalcogenide glasses near the rigidity

15512916, 2026, 11, Downloaded from https://ceramics.onlinelibrary.wiley.com/doi/10.1111/jace.71368 by University Of Sheffield, Wiley Online Library on [03/11/2026]. See the Terms and Conditions (https://onlinelibrary.wiley.com/terms-and-conditions) on Wiley Online Library for rules of use; OA articles are governed by the applicable Creative Commons License

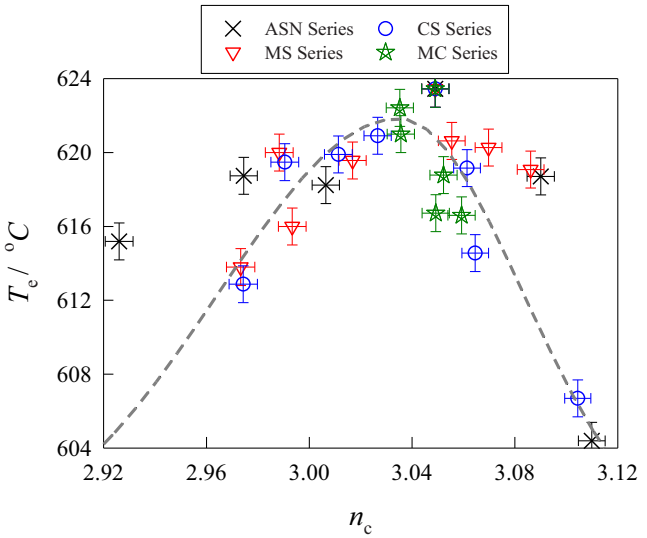


FIGURE 6 | Variation of T_e with n_c in the studied glasses during structural relaxation.

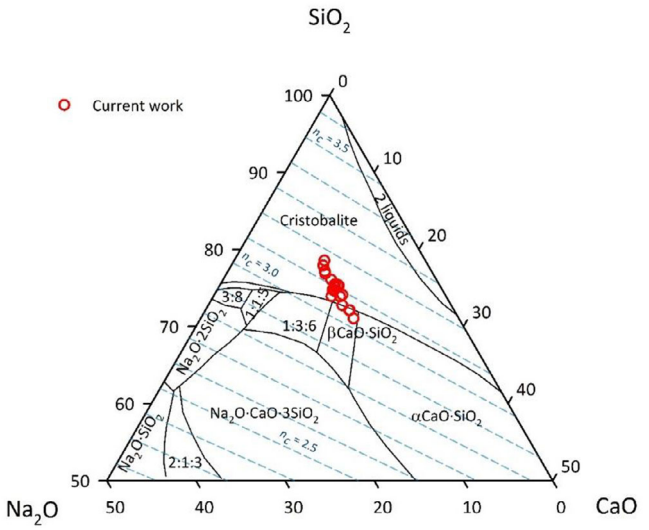


FIGURE 7 | SiO_2 includes SiO_2 plus charge-balanced Al_2O_3, CaO includes CaO plus MgO, and Na_2O represents the excess alkali after subtracting that required for Al^{3+} charge compensation.

transition [5, 58, 59]. Consistent with these findings, our study shows that T_e reaches a maximum near n_c = 3.04, suggesting that T_e obtained from the reheating cycle serves as a sensitive indicator of structural rearrangements in quinary silicate glasses, peaking within the isostatic phase field. Moreover, the observed association between T_e and n_c across the studied 25 glass compositions examined is in close agreement with topological constraint theory, wherein the onset of ergodicity breakdown during structural relaxation, reflected in T_e, is likely governed by the number of rigid constraints within the network [60].

3.7 | Ideal Soda-Lime-Silicate Glass Compositions

Bauchy et al. [14] reported inversions or step changes in the modeled brittleness and fracture toughness of various types of glasses at n_c values of approximately 2.8 and 3.2. Our experimental study of soda-lime-silicate glasses reveals similar characteristics, with minima in static fatigue and brittleness, together with elevated onset temperatures of the glass transition during cooling, consistently observed in the vicinity of n_c = 3.00–3.06. Similarly, the most favorable glass properties—particularly those associated with a minimum or moderately elevated liquidus temperature—are generally observed within the n_c = 3.00–3.06 range, where soda-lime-silicate glasses favor an isostatic network configuration (Figure 5).

Our research also indicates the concurrent influence of other topologically relevant criteria on the material properties of soda-lime-silicate glasses, beyond n_c alone. Figure 4 highlights the glasses positioned at $n_c \approx 3.06$, where several Raman-derived topological property inversions coincide, as indicated by the color-coded data points. These glasses are characterized by a predominance of $m \approx 6$ ring motifs and well-balanced ν_H/ν_M ratios ranging from 1.3925 to 1.3955. This intersection suggests that favorable glass properties are associated with topological domains in which the isostatically favorable n_c and ν_H/ν_M coincide with a greater fraction of ~ six-membered ring motifs. Furthermore, superimposition of the studied compositions and their corresponding n_c values onto the SiO_2-Na_2O-CaO ternary phase diagram, as shown in Figure 7, indicates that glasses exhibiting favorable combinations of n_c, ring statistics, and ν_H/ν_M tend to cluster near a crystalline phase boundary. Specifically, these compositions are located near the transition between the β-$CaO \cdot SiO_2$ and cristobalite phase fields, or vice versa.

Moreover, good glass-forming ability and superior crystallization resistance in both inorganic and metallic glasses have been correlated with higher T_g/T_L values [61–63]. In line with this, glasses that exhibit favorable Raman ν_H/ν_M values and ring statistics associated with optimal crystallization and mechanical properties also show some of the highest T_e/T_L values among the studied glass series, with T_g replaced by T_e for this analysis. The observed correlation between glass properties and topological events suggests that T_e may have potential as a topological metric. The elevated T_e values suggest that glass formation in these compositions may initiate earlier within the supercooled-liquid region, potentially enhancing their overall structural stability.

Overall, these findings suggest that the synergistic effects of topological events—interpreted within the framework of mechanical trusses—can outweigh the conventional role of glass chemistry, at least at the molecular level, and exert a dominant influence on the properties of silicate glasses. The corresponding ideal glass compositions within this domain, together with the contributions of their individual oxide components, will be presented and discussed in a separate publication.

3.8 | Novel Glass Composition Design

It is plausible that multiple compositional arrays exist within the soda-lime-silicate glass system where the desired properties can be achieved. Beyond the topological criterion of ring-size distribution and n_c, the spectral rigidity transition constant, ν_H/ν_M, may serve as a complementary and valuable metric for further refining isostatically favorable glass compositions along

15512916, 2026, 11, Downloaded from https://ceramics.onlinelibrary.wiley.com/doi/10.1111/jace.71368 by University Of Sheffield, Wiley Online Library on [03/11/2026]. See the Terms and Conditions (https://onlinelibrary.wiley.com/terms-and-conditions) on Wiley Online Library for rules of use; OA articles are governed by the applicable Creative Commons License

a given compositional array. However, at the current stage, this Raman processing pathway may only be applicable to SiO_2-based glass systems, including alkali and alkaline-earth silicate glasses and aluminosilicate systems (Na_2O-$Al_2O_3 > 0$ in mol.%), where the resulting network structures exhibit Raman spectral fingerprints and vibrational characteristics comparable to those of archetypal soda-lime-silicate glasses. This refinement could help narrow down experimental sets to a manageable number, ultimately aiding in the development of commercially viable glasses with optimal crystallization and mechanical properties.

4 | Conclusion

Our experimental study provides a further demonstration that topological constraint theory can be extended to quinary silicate and soda-lime-silica glass systems. However, the boundaries of the isostatic field appear sufficiently broad to accommodate a range of theoretically ideal silicate glass networks derived from diverse glass chemistries. Moreover, our analysis suggests that the n_c may not fully capture the impact of certain nanoscale phenomena within the atomic topology of glasses, and therefore it may not alone serve as a reliable predictor for identifying promising glass compositions tailored to specific functionalities. Our exploratory analysis indicates that the theoretical framework proposed by Phillips and Kernel [9], which emphasizes the critical role of $m \approx 6$ ring motifs, together with our established spectral rigidity transition parameter (ν_H/ν_M), can serve as complementary metrics for refining the identification of truly isostatic glass compositions within the broader theoretical isostatic domain. This integrated approach may offer a pathway for designing glasses with optimized topological, processing, and functional properties, and can be applied across diverse design frameworks to engineer glass compositions ranging from low-carbon commercial soda-lime-silicate glasses to complex formulations for aluminosilicate glasses.

Funding

The authors have nothing to report.

Conflicts of Interest

The authors declare no conflicts of interest.

Data Availability Statement

The data that support the findings of this study are available on request from the corresponding author. The data are not publicly available due to privacy or ethical restrictions.

References

1. J. C. Mauro, A. J. Ellison, D. C. Allan, and M. M. Smedskjaer, "Topological Model for the Viscosity of Multicomponent Glass-Forming Liquids," *International Journal of Applied Glass Science* 4, no. 4 (2013 December): 408–413.

2. S. Gin, M. Wang, N. Bisbrouck, et al., "Can a Simple Topological-Constraints-Based Model Predict the Initial Dissolution Rate of Borosilicate and Aluminosilicate glasses?," *npj Materials Degradation* 4, no. 1 (2020 March): 6.

3. J. C. Mauro, *Topological Constraint Theory of Glass* (American Ceramic Society Bulletin, 2011 May), 31.

4. K. Januchta, R. E. Youngman, A. Goel, et al., "Discovery of Ultra-Crack-Resistant Oxide Glasses With Adaptive Networks," *Chemistry of Materials* 29, no. 14 (2017 July): 5865–5876.

5. B. H. Sharmila, J. T. Devaraju, and S. Asokan, "A Modulated Differential Scanning Calorimetric Study of As-Te-In Glasses," *Journal of Non-Crystalline Solids* 326 (2003 October): 154–158.

6. G. S. Varma, C. Das, and S. Asokan, "Evidence of an Intermediate Phase in a Quaternary Ag Bearing Telluride Glass System Using Alternating DSC," *Solid State Communications* 177 (2014 January): 108–112.

7. J. Kjeldsen, M. M. Smedskjaer, J. C. Mauro, R. E. Youngman, L. Huang, and Y. Yue, "Mixed Alkaline Earth Effect in Sodium Aluminosilicate Glasses," *Journal of Non-Crystalline Solids* 369 (2013 June): 61–68.

8. T. Abe, "Borosilicate Glasses," *Journal of the American Ceramic Society* 35, no. 11 (1952 November): 284–299.

9. J. C. Phillips and R. Kerner, "Structure and Function of Window Glass and Pyrex," *Journal of chemical physics* 128, no. 17 (2008 May): 174506.

10. M. M. Smedskjaer, R. E. Youngman, and J. C. Mauro, "Principles of Pyrex® Glass Chemistry: Structure–Property Relationships," *Applied Physics A* 116 (2014 August): 491–504.

11. A. Yadav, A. Rebecca, S. Kapoor, Y. T. Shih, L. Huang, and A. Goel, "Structural Design of a Scalable Glass With High Hardness and Crack Initiation Resistance," *Materials Today* 78 (2024 September): 1–9.

12. R. Kerner and J. C. Phillips, "Quantitative Principles of Silicate Glass Chemistry," *Solid State Communications* 117, no. 1 (2000 November): 47–51.

13. M. M. Smedskjaer, J. C. Mauro, and Y. Yue, "Ionic Diffusion and the Topological Origin of Fragility in Silicate Glasses," *Journal of Chemical Physics* 131, no. 24 (2009 December): 244514.

14. M. Bauchy, B. Wang, M. Wang, et al., "Fracture Toughness Anomalies: Viewpoint of Topological Constraint Theory," *Acta Materialia* 121 (2016 December): 234–239.

15. Y. Vaills, T. Qu, M. Micoulaut, F. Chaimbault, and P. Boolchand, "Direct Evidence of Rigidity Loss and Self-Organization in Silicate Glasses," *Journal of Physics: Condensed Matter* 17, no. 32 (2005 July): 4889.

16. S. Karlsson, "Viscosity of Alumina Doped Soda Lime Silicate Glasses-Observation of Anomaly in the Linear Increase as Al_2O_3 Replaces SiO_2," *Journal of Non-Crystalline Solids* 573 (2021 December): 121149.

17. R. Gy, "Stress Corrosion of Silicate Glass: A Review," *Journal of Non-Crystalline Solids* 316, no. 1 (2003 February): 1.

18. T. Rouxel, "Driving Force for Indentation Cracking in Glass: Composition, Pressure and Temperature Dependence," *Philosophical Transactions of the Royal Society A: Mathematical, Physical and Engineering Sciences* 373, no. 2038 (2015 March 28): 20140140.

19. S. Wiederhorn and L. H. Bolz, "Stress Corrosion and Static Fatigue of Glass," *Journal of the American Ceramic Society* 53, no. 10 (1970 October): 543–548.

20. S. Dériano, A. Jarry, T. Rouxel, J. C. Sangleboeuf, and S. Hampshire, "The Indentation Fracture Toughness (KC) and Its Parameters: The Case of Silica-Rich Glasses," *Journal of Non-Crystalline Solids* 344, no. 1-2 (2004 September): 44–50.

21. T. Waurischk, R. Müller, H. Behrens, and J. Deubener, "Crack Growth in Borate and Silicate Glasses: Stress-Corrosion Susceptibility and Hydrolytic Resistance," *Journal of Non-Crystalline Solids* 551 (2021 January): 120414.

22. E. Kilinc and R. J. Hand, "Mechanical Properties of Soda-Lime-Silica Glasses With Varying Alkaline Earth Contents," *Journal of Non-Crystalline Solids* 429 (2015 December): 190–197.

23. E. Kilinc, A. M. Bell, P. A. Bingham, and R. J. Hand, "Effects of Composition and Phase Relations on Mechanical Properties and

15512916, 2026, 11, Downloaded from https://ceramics.onlinelibrary.wiley.com/doi/10.1111/jace.71368 by University Of Sheffield, Wiley Online Library on [03/11/2026]. See the Terms and Conditions (https://onlinelibrary.wiley.com/terms-and-conditions) on Wiley Online Library for rules of use; OA articles are governed by the applicable Creative Commons License

Crystallization of Silicate Glasses," *Journal of the American Ceramic Society* 104, no. 8 (2021 August): 3921–3946.

24. Q. Zhou, Y. Shi, B. Deng, J. Neuefeind, and M. Bauchy, "Experimental Method to Quantify the Ring Size Distribution in Silicate Glasses and Simulation Validation Thereof," *Science Advances* 7, no. 28 (2021 July): eabh1761.

25. S. K. Sharma, J. A. Philpotts, and D. W. Matson, "Ring Distributions in Alkali- and Alkaline-Earth Aluminosilicate Framework Glasses—A Raman Spectroscopic Study," *Journal of Non-Crystalline Solids* 71, no. 1-3 (1985 May 1): 403–410.

26. K. Awazu, K. Sasa, and A. Uedono, "Ring-Size Reconstruction and Damage Morphology in Silica Glass Under Swift Heavy-Ion Irradiation," *Journal of Non-Crystalline Solids* 679 (2026 April): 124027.

27. M. Cassetta, D. Szewczyk, G. Giuliani, et al., "Chemically Driven Nano-Elastic Heterogeneities Control Fragility in Volcanic Melts," *Advanced Science* 13, no. 5 (2026 January): e12063.

28. Z. Pan, O. Benzine, S. Sawamura, et al., "Disorder Classification of the Vibrational Spectra of Modern Glasses," *Physical Review B* 104, no. 13 (2021 October): 134106.

29. O. Laurent, B. Mantisi, and M. Micoulaut, "Structure and Topology of Soda-Lime Silicate Glasses: Implications for Window Glass," *Journal of Physical Chemistry B* 118, no. 44 (2014 November): 12750–12762.

30. T. Rouxel and S. Yoshida, "The Fracture Toughness of Inorganic Glasses," *Journal of the American Ceramic Society* 100, no. 10 (2017 October): 4374–4396.

31. M. I. Ojovan, "Viscosity and Glass Transition in Amorphous Oxides," *Advances in Condensed Matter Physics* 2008, no. 1 (2008): 817829.

32. H. Liu, T. Zhang, M. M. Smedskjaer, J. V. Ryan, S. Gin, and M. Bauchy, "Predicting the Dissolution Kinetics of Silicate Glasses by Topology-Informed Machine Learning," *Npj Materials Degradation* 3, no. 1 (2019 August): 32.

33. E. Ching and M. Bauchy, "Topological Origins of Flexibility and Internal Stress in Sodium Aluminosilicate Glasses. arXiv: Materials Science. arXiv:1812.04791," (2018 December).

34. P. McMillan, "Structural Studies of Silicate Glasses and Melts-Applications and Limitations of Raman Spectroscopy," *American Mineralogist* 69, no. 7-8 (1984 August): 622–644.

35. F. Barmes, L. Soulard, and M. Mareschal, "Molecular Dynamics of Shock-Wave Induced Structural Changes in Silica Glasses," *Physical Review B* 73, no. 22 (2006 June): 224108.

36. M. Shiga, A. Hirata, Y. Onodera, and H. Masai, "Ring-Originated Anisotropy of Local Structural Ordering in Amorphous and Crystalline Silicon Dioxide," *Communications Materials* 4, no. 1 (2023 November): 91.

37. H. Liu, H. Kaya, Y. T. Lin, A. Ogrinc, and S. H. Kim, "Vibrational Spectroscopy Analysis of Silica and Silicate Glass Networks," *Journal of the American Ceramic Society* 105, no. 4 (2022 April): 2355–2384.

38. C. Le Losq, D. R. Neuville, P. Florian, G. S. Henderson, and D. Massiot, "The Role of Al3+ on Rheology and Structural Changes in Sodium Silicate and Aluminosilicate Glasses and Melts," *Geochimica et Cosmochimica Acta* 126 (2014 February): 495–517.

39. S. Ito, T. Taniguchi, M. Ono, and K. Uemura, "Network and Void Structures for Glasses With a Higher Resistance to Crack Formation," *Journal of Non-Crystalline Solids* 358, no. 24 (2012 December): 3453–3458.

40. T. Furukawa, K. E. Fox, and W. B. White, "Raman Spectroscopic Investigation of the Structure of Silicate Glasses. III. Raman Intensities and Structural Units in Sodium Silicate Glasses," *Journal of Chemical Physics* 75, no. 7 (1981 October): 3226–3237.

41. F. L. Galeener, "Band Limits and the Vibrational Spectra of Tetrahedral Glasses," *Physical Review B* 19, no. 8 (1979 April): 4292.

42. M. Micoulaut, M. Malki, P. Simon, and A. Canizares, "On the Rigid to Floppy Transitions in Calcium Silicate Glasses From Raman Scattering and Cluster Constraint Analysis," *Philosophical Magazine* 85, no. 28 (2005 October): 3357–3378.

43. G. S. Henderson, G. M. Bancroft, M. E. Fleet, and D. J. Rogers, "Raman Spectra of Gallium and Germanium Substituted Silicate Glasses: Variations in Intermediate Range Order," *American Mineralogist* 70, no. 9-10 (1985 October): 946–960.

44. P. Boolchand, X. Feng, and W. J. Bresser, "Rigidity Transitions in Binary Ge–Se Glasses and the Intermediate Phase," *Journal of Non-Crystalline Solids* 293 (2001 November): 348–356.

45. K. Yang, Y. Hu, Z. Li, et al., "Analytical Model of the Network Topology and Rigidity of Calcium Aluminosilicate Glasses," *Journal of the American Ceramic Society* 104, no. 8 (2021 August): 3947–3962.

46. M. Wang, B. Wang, T. K. Bechgaard, et al., "Crucial Effect of Angular Flexibility on the Fracture Toughness and Nano-Ductility of Aluminosilicate Glasses," *Journal of Non-Crystalline Solids* 454 (2016 December): 46–51.

47. G. W. Morey, "The Devitrification of Soda-Lime-Silica Glasses 1," *Journal of the American Ceramic Society* 13, no. 10 (1930 October): 683–713.

48. W. B. Silverman, "Effect of Alumina on Devitrification of Soda-Lime-Silica Glasses," *Journal of the American Ceramic Society* 22, no. 1-12 (1939 December): 378–384.

49. W. B. Silverman, "Effect of Alumina on Devitrification of Sodium Oxide-Dolomite Lime-Silica Glasses," *Journal of the American Ceramic Society* 23, no. 9 (1940): 274–281.

50. F. T. Wallenberger, R. J. Hicks, and A. T. Bierhals, "Design of Environmentally Friendly Fiberglass Compositions: Ternary Eutectic SiO_2-Al_2O_3-CaO Compositions, Structures and Properties," *Journal of Non-Crystalline Solids* 349 (2004 December): 377–387.

51. P. Hrma, D. E. Smith, J. Matyáš, J. D. Yeager, J. V. Jones, and E. N. Boulos, "Effect of Float Glass Composition on Liquidus Temperature and Devitrification Behaviour," *Physics and Chemistry of Glasses-European Journal of Glass Science and Technology Part B* 47, no. 1 (2006 February): 64–76.

52. F. T. Wallenberger and A. Smrček, "The Liquidus Temperature; Its Critical Role in Glass Manufacturing," *International Journal of Applied Glass Science* 1, no. 2 (2010 June): 151–163.

53. B. M. Abel, J. C. Mauro, M. M. Smedskjaer, et al., "Liquidus Surface of MgO-CaO-Al_2O_3-SiO_2 Glass-forming Systems," *Journal of Non-Crystalline Solids* 363 (2013 March): 39–45.

54. E. Kilinc, A. M. Bell, and P. A. Bingham, "Dynamic High-temperature Crystallization and Processing Properties of Industrial Soda-Lime-Silica Glasses," *Journal of the American Ceramic Society* 107, no. 4 (2024 April): 2242–2259.

55. J. C. Phillips, "Topology of Covalent Non-Crystalline Solids I: Short-Range Order in Chalcogenide Alloys," *Journal of Non-Crystalline Solids* 34, no. 2 (1979 October): 153–181.

56. M. Micoulaut, "Linking Rigidity Transitions With Enthalpic Changes at the Glass Transition and Fragility: Insight From a Simple Oscillator Model," *Journal of Physics: Condensed Matter* 22, no. 28 (2010 June): 285101.

57. M. Bauchy and M. Micoulaut, "Densified Network Glasses and Liquids With Thermodynamically Reversible and Structurally Adaptive Behaviour," *Nature Communications* 6, no. 1 (2015 March): 6398.

58. M. Tatsumisago, B. L. Halfpap, J. L. Green, S. M. Lindsay, and C. A. Angell, "Fragility of Ge-As-Se Glass-Forming Liquids in Relation to Rigidity Percolation, and the Kauzmann Paradox," *Physical Review Letters* 64, no. 13 (1990 March): 1549.

59. M. Zhang, S. Mancini, W. Bresser, and P. Boolchand, "Variation of Glass Transition Temperature, Tg, With Average Coordination Number, < M >, in Network Glasses: Evidence of a Threshold Behavior in the Slope | dTg /D <M>| at the Rigidity Percolation Threshold (< m >= 2.4)," *Journal of Non-Crystalline Solids* 151, no. 1-2 (1992 December): 149–154.

15512916, 2026, 11, Downloaded from https://ceramics.onlinelibrary.wiley.com/doi/10.1111/jace.71368 by University Of Sheffield, Wiley Online Library on [03/11/2026]. See the Terms and Conditions (https://onlinelibrary.wiley.com/terms-and-conditions) on Wiley Online Library for rules of use; OA articles are governed by the applicable Creative Commons License

60. J. C. Mauro and M. M. Smedskjaer, "Statistical Mechanics of Glass," *Journal of Non-Crystalline Solids* 396 (2014 August): 41–53.

61. I. Avramov, E. D. Zanotto, and M. O. Prado, "Glass-Forming Ability Versus Stability of Silicate Glasses. II. Theoretical Demonstration," *Journal of Non-Crystalline Solids* 320, no. 1-3 (2003 June): 9–20.

62. E. D. Zanotto and V. M. Fokin, "Recent Studies of Internal and Surface Nucleation in Silicate Glasses," *Philosophical Transactions of the Royal Society of London Series A: Mathematical, Physical and Engineering Sciences* 361, no. 1804 (2003 March): 591–613.

63. Y. Zhang, Y. Li, H. Tan, and G. L. Chen, "Effect of Liquidus Temperature Depression on Glass Forming Ability Criteria for La-Al- (Cu, Ni) alloys," *Intermetallics* 15, no. 5-6 (2007 May): 744–748.

15512916, 2026, 11, Downloaded from https://ceramics.onlinelibrary.wiley.com/doi/10.1111/jace.71368 by University Of Sheffield, Wiley Online Library on [03/11/2026]. See the Terms and Conditions (https://onlinelibrary.wiley.com/terms-and-conditions) on Wiley Online Library for rules of use; OA articles are governed by the applicable Creative Commons License